Supporting Information

Shaping and Edge Engineering of Few-Layered Freestanding Graphene Sheets in a Transmission Electron Microscope

*Longze Zhao[#1], Guangfu Luo[#2], Yong Cheng[1] , Xin Li[1], Shiyuan Zhou[3], Chenxu Luo[3], Jinming Wang[1], Hong-Gang Liao[3], Dmitri Golberg[4,5], Ming-Sheng Wang[1]**

[1] Department of Materials Science and Engineering, College of Materials, and Pen-Tung Sah Institute of Micro-Nano Science and Technology, Xiamen University, Xiamen, Fujian 361005, China.

[2] Department of Materials Science and Engineering, Southern University of Science and Technology, Shenzhen, Guangdong 518055, China.

[3] State Key Lab of Physical Chemistry of Solid Surfaces, Collaborative Innovation Center of Chemistry for Energy Materials, College of Chemistry and Chemical Engineering, Xiamen University, Xiamen, 361005, P. R. China

[4] School of Chemistry, Physics and Mechanical Engineering, Science and Engineering Faculty, Queensland University of Technology (QUT), 2nd George str., Brisbane, QLD 4000, Australia

[5] International Center for Materials Nanoarchitectonics (MANA), National Institute for Materials Science (NIMS), Namiki 1-1, Tsukuba, Ibaraki 3050044, Japan

*Address correspondence to: mswang@xmu.edu.cn

[#] These authors contributed equally to this work

Supplementary Figures

Figure S1-S11

Supplementary Tables

Table S1

Supplementary Movies

Movie S1-S3

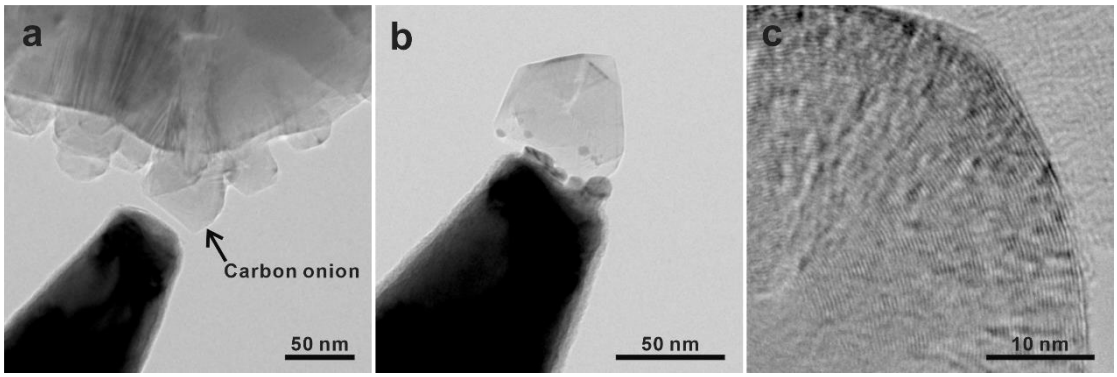

Figure S1. The preparation of a tool tip capped with a carbon "onion" as the cutting edge. TEM images of a tungsten tip and a carbon onion (a) before and (b) after their nanowelding. (c) HRTEM image of the carbon onion.

Before the graphene tailoring experiment, a small piece of graphitic carbon was deliberately welded onto the end of a tungsten tip to fabricate the machine tool tip for tailoring. In this case, a tool tip with a carbon onion as the cutting edge was fabricated by touching the carbon onion with the W tip under a constant bias of 1-2 V (Figure S1), resulting in their nanowelding.

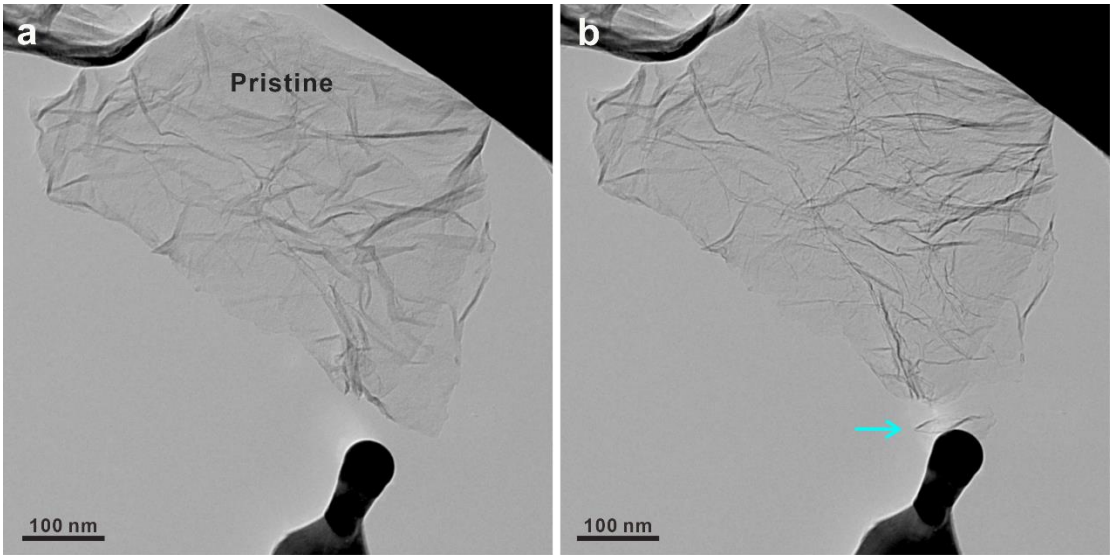

Figure S2. The preparation of a tool tip capped with a small graphene fragment as the cutting edge. The RGO sheet before (a) and after (b) the electrical breakdown by touching it with a biased tip.

In order to fabricate a tool tip capped with a small graphene fragment as the cutting edge, we applied an appropriate bias (2.0~3.0 V) on a clean W tip and moved it close to the edge of a large RGO sheet (Figure S2a). A small graphene fragment was removed from the RGO sheet and welded onto the W tip-end due to the electrical breakdown of RGO, as indicated by the blue arrow in Figure S2b.

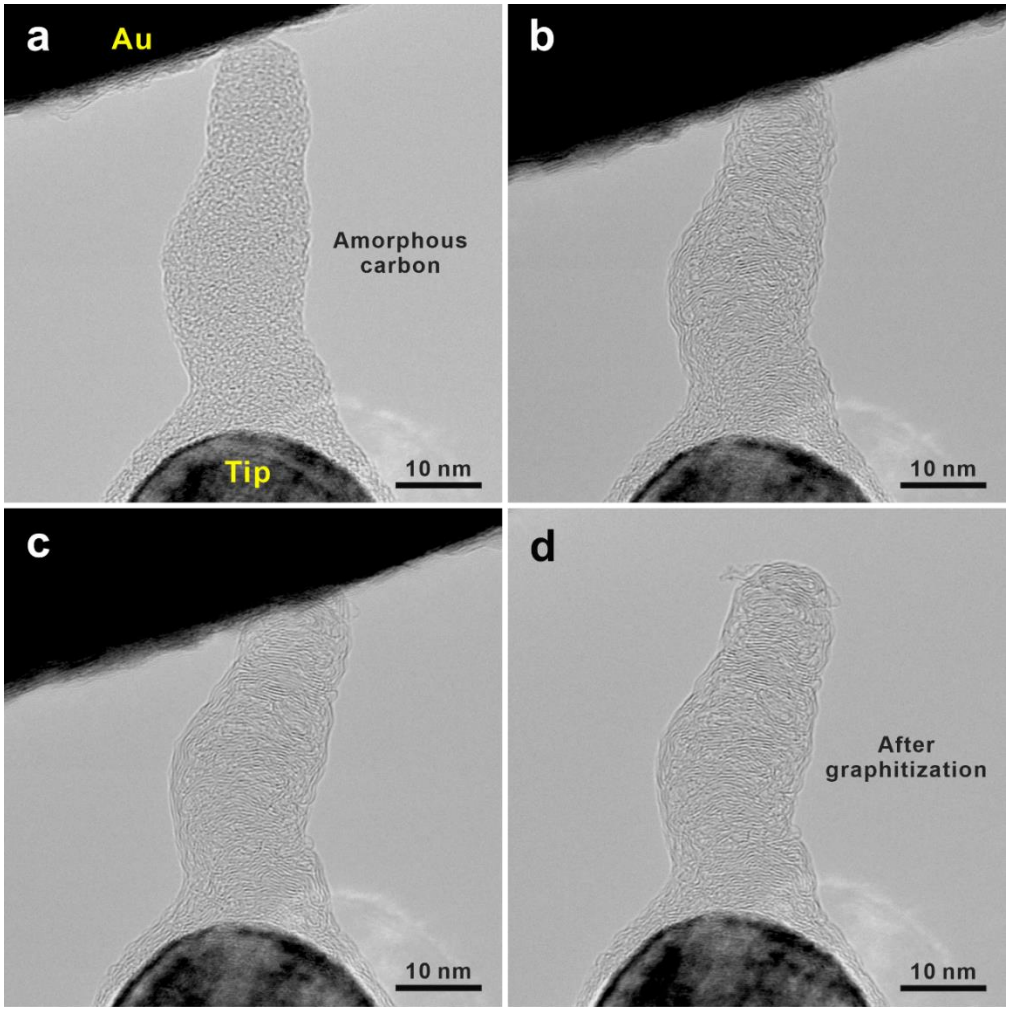

Figure S3. The preparation of a tool tip with graphitized amorphous carbon as the cutting edge. (a) TEM image of amorphous carbon deposited on the W tip by electron beam induced deposition (EBID). (b,c) Structural evolution of the carbon deposit during a controlled Joule heating process. (d) The tool tip after the graphitization of the amorphous carbon deposit.

Another way to prepare a tool tip is the deposition of amorphous carbon on the tip-end by electron beam induced deposition (EBID) (Figure S3a), followed by its graphitization *via* a controlled Joule heating process by passing through a high current (Figure S3b, c). In this way, we can produce a tool tip with a graphitized amorphous carbon deposit as the cutting edge (Figure S3d), which is much more robust upon graphene etching compared to its amorphous counterpart.

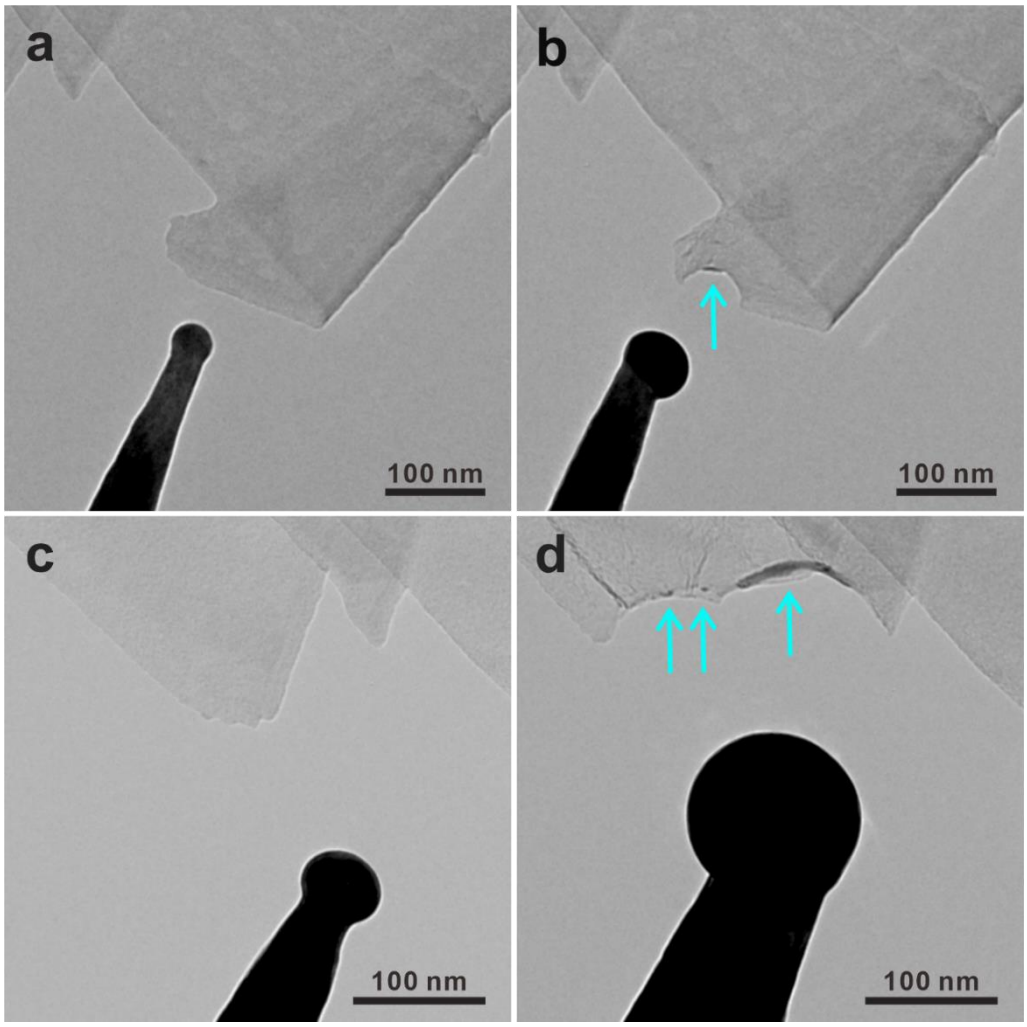

Figure S4. **Two sets of tailoring attempts using bare tungsten tips as the cutting tool.** TEM images of the graphene sheets (a,c) before and (b,d) after the tailoring attempts. The blue arrows indicate the W species residual on the graphene edges.

Figure S4 shows a series of tailoring attempts using a bare tungsten tip as the tool tip without the protection of graphitic carbon. It can be found that the W tips were easily melted and deformed to form a ball-like tip end with larger size after tailoring, as shown in Figures S4b and 4d. In the meantime, some W species (possibly tungsten carbides) from the tips were left behind on the freshly-formed graphene edges, as indicated by the blue arrows.

Actually, the bare tungsten tips can also be viewed as a material to be etched, and the graphene sheets as the cutting edge. The tip having sole metallic bonds behaves quite differently from graphene/CNTs constructed from covalent C-C bonds. The breakage of C-C bonds leads to the evaporation and removal of carbon atoms from graphene/CNTs. Instead, weakening of the metallic bonds caused by tunneling currents tends to cause metal melting. Tungsten atoms can diffuse along the tip surface, leading to the ball-like morphology of the tip end, with a small fraction of W atoms emitted and accumulated on the edge of graphene. That is why, using our method, it is difficult to tailor tungsten in a controlled way and to form a desired morphology. We also assume that this conclusion might be true for other metals as well (however, more experiments are needed to verify this).

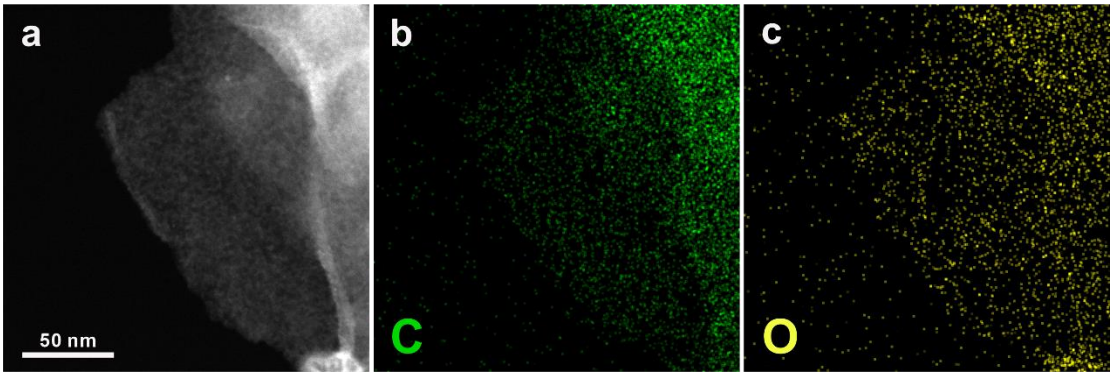

Figure S5. (a) High-angle annular dark field (HAADF) image of a reduced graphene oxide (RGO) sheet and (b,c) the corresponding C and O EDS elemental maps.

Table S1. Quantification of oxygen in RGO by EDS.

Element	Atomic Fraction (%)	Atomic Error (%)
C	89.40	4.28
O	10.60	2.19

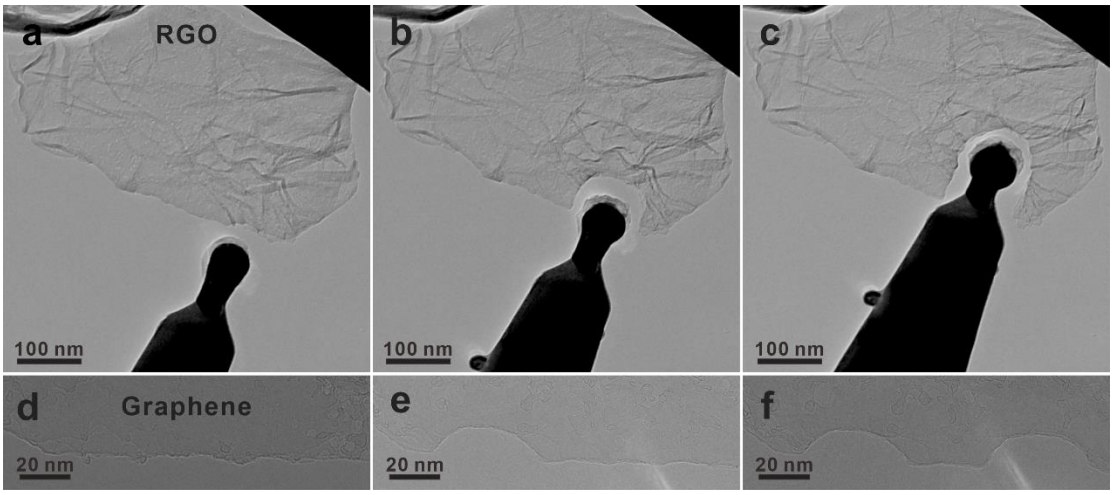

Figure S6. Two typical cases of graphene sheets with irregular architectures. (a-c) Carving a notch inward from the edge of a RGO sheet with varied depths. (d-f) Creating two curved edge domains on the initially straight edge of a pure graphene sheet.

Our method theoretically allows the edge formation along any directions or irregular cutting trajectories, thus providing high flexibility and processing accuracy for graphene architecture design. Many complicated graphene shapes can be obtained using our method. Figure S6 shows two examples of such graphene sheets. Under careful manipulation, we can make a U-shaped notch with different depths on the edge of a RGO sheet (Figures S6b,c), or create two curved edge domains on the initially straight edge of a pure graphene sheet (Figures S6e,f).

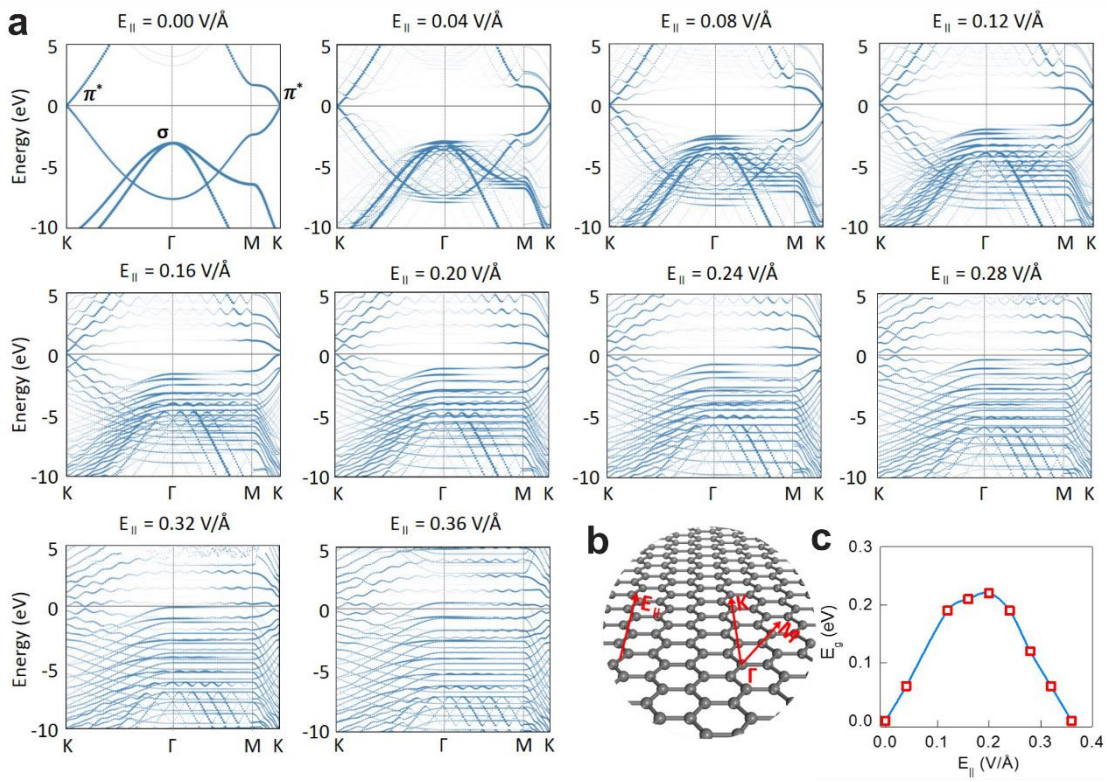

Figure S7. Full result of the band structure of graphene by first-principles calculations. (a) Computational band structures of graphene under different in-plane electric fields. The band structures are unfolded to the Brillouin zone of primitive cell of graphene; Fermi level is set to zero. (b) Honeycomb lattice of graphene indicating the direction of electric field and high-symmetry *k*-points. (c) Band gap (E_g) of graphene under the increasing in-plane electric fields from 0 to 0.36 V/Å.

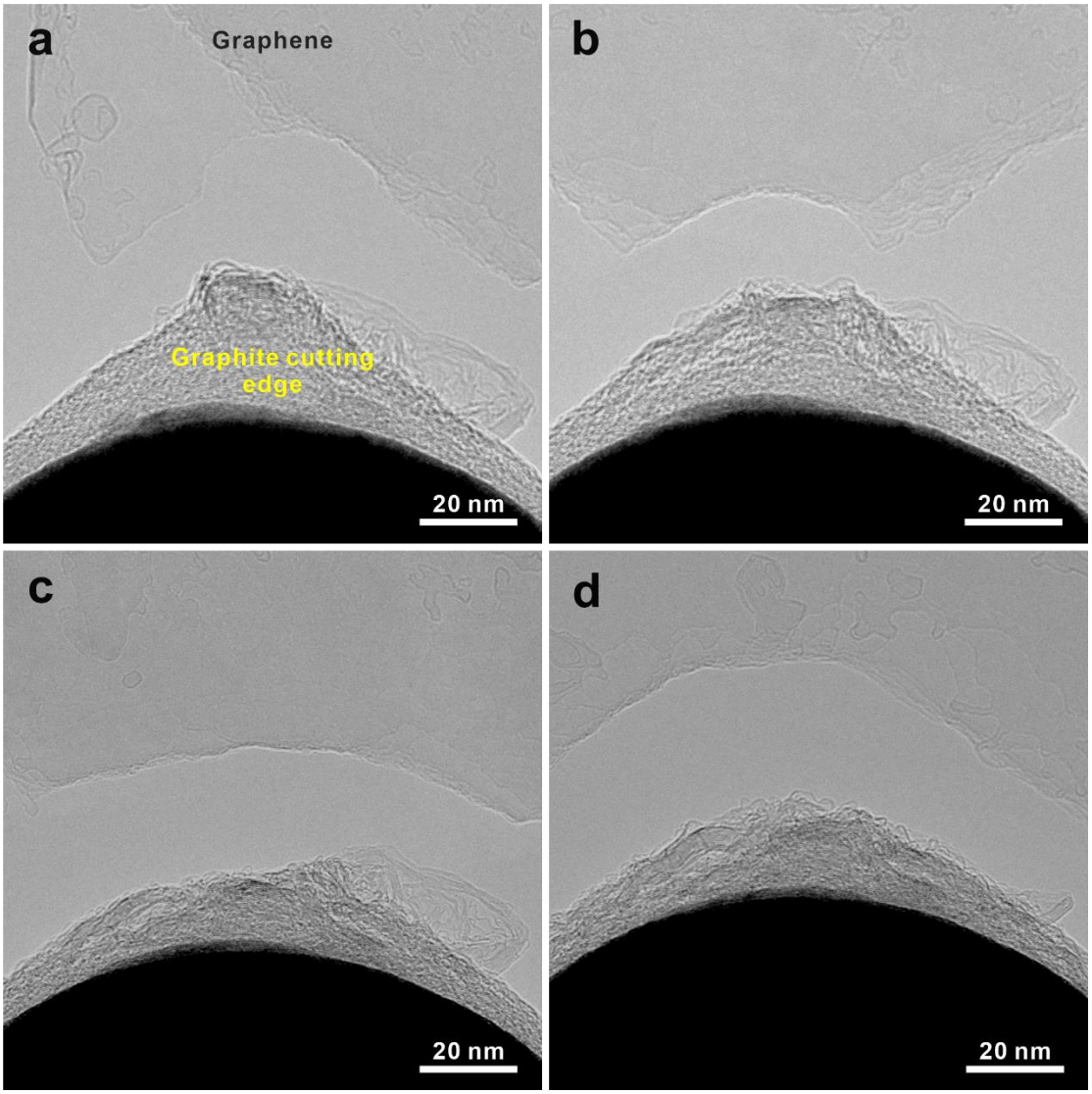

Figure S8. The gradual wear of the graphite cutting edge during repeated graphene etching. (a-d) Structural evolution of the graphite cutting edge that was gradually etched and deformed during the wear process.

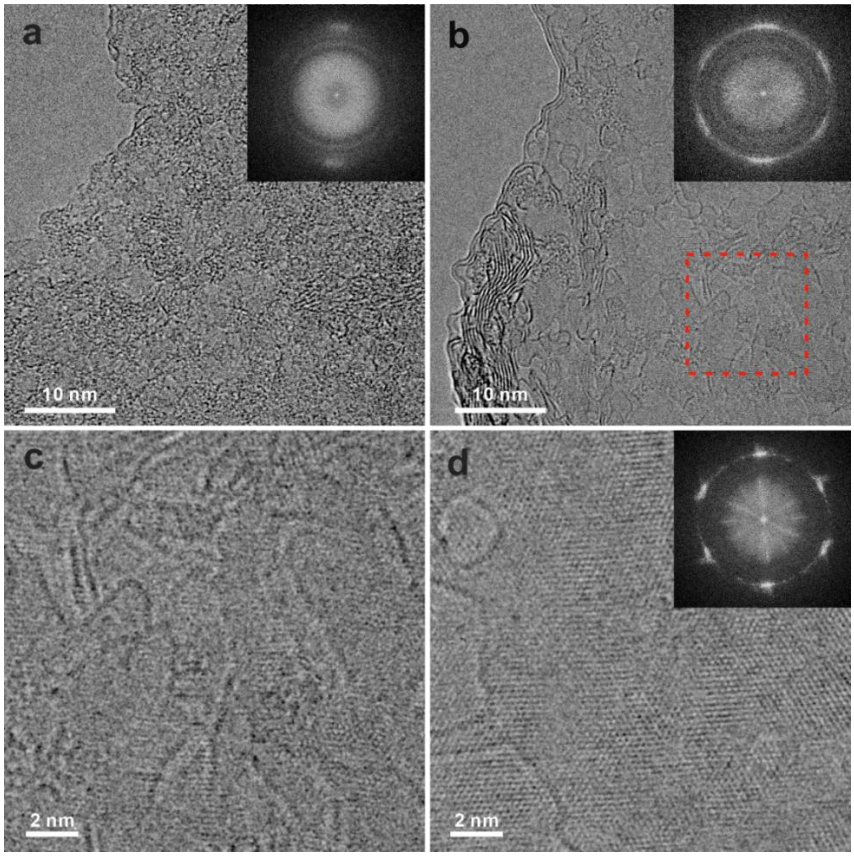

Figure S9. Evolution of the crystallinity of a RGO sheet during *in situ* Joule heating. TEM images of the RGO sheet (a) before and (b) after *in situ* annealing. The insets are the corresponding FFT patterns. (c) HRTEM image of the graphene domain marked in (b). (d) The same graphene domain with further improved crystallinity after prolonged annealing, as can be revealed from the corresponding FFT pattern (inset).

For RGO sheets with poor crystallinity, as that in Figure S9a, a simple *in situ* heat treatment can be employed to get clearer FFT/SAED patterns or HRTEM lattice fringes required for a crystallographic tailoring. It can be confirmed from both the FFT patterns and HRTEM images that the graphene crystallinity was gradually improved during *in situ* heating. The six FFT $\{1\bar{1}00\}$ reflexes become clearer and sharper (insets), and the lattice fringes get more ordered after annealing.

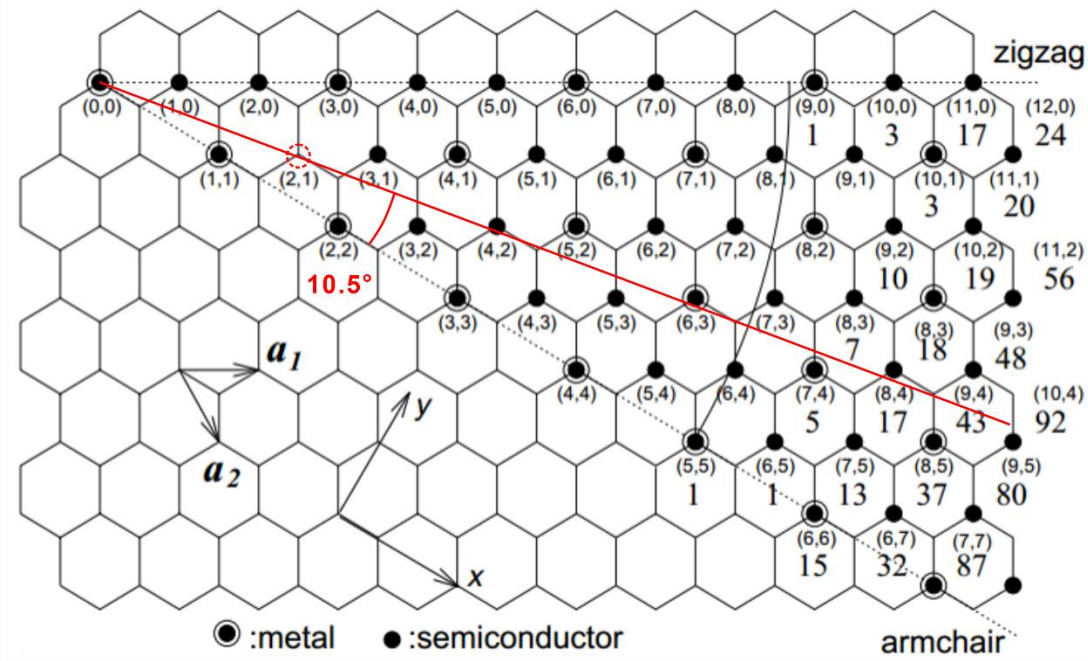

Figure S10. The chiral vector (n, m) is defined on the honeycomb lattice of carbon atoms by unit vectors $\boldsymbol{a}_1$ and $\boldsymbol{a}_2$ and the chiral angle θ with respect to the zigzag axis.[1] The red circle highlights the (2, 1) chiral vector.

According to the definition in reference [1], the chiral angle θ is given by:

$$\theta = \tan^{-1}[\sqrt{3}m/(2n+m)] \qquad (1)$$

It follows that $\theta = 0°$ for the (n, 0) zigzag direction and $\theta = 30°$ for the (n, n) armchair direction. The red line in the Figure S10 indicates the edge orientation obtained by tailoring in Figure 4d. It forms an angle of 10.5° with respect to the armchair direction, corresponding to the chiral angle of $\theta = 19.5°$, which is very close to the (2, 1) direction ($\theta = 19.1°$). Therefore, we can assume that the obtained edge in Figure 4d is approximately oriented along the (2n, n) chiral direction in the honeycomb lattice, as mentioned in the main text.

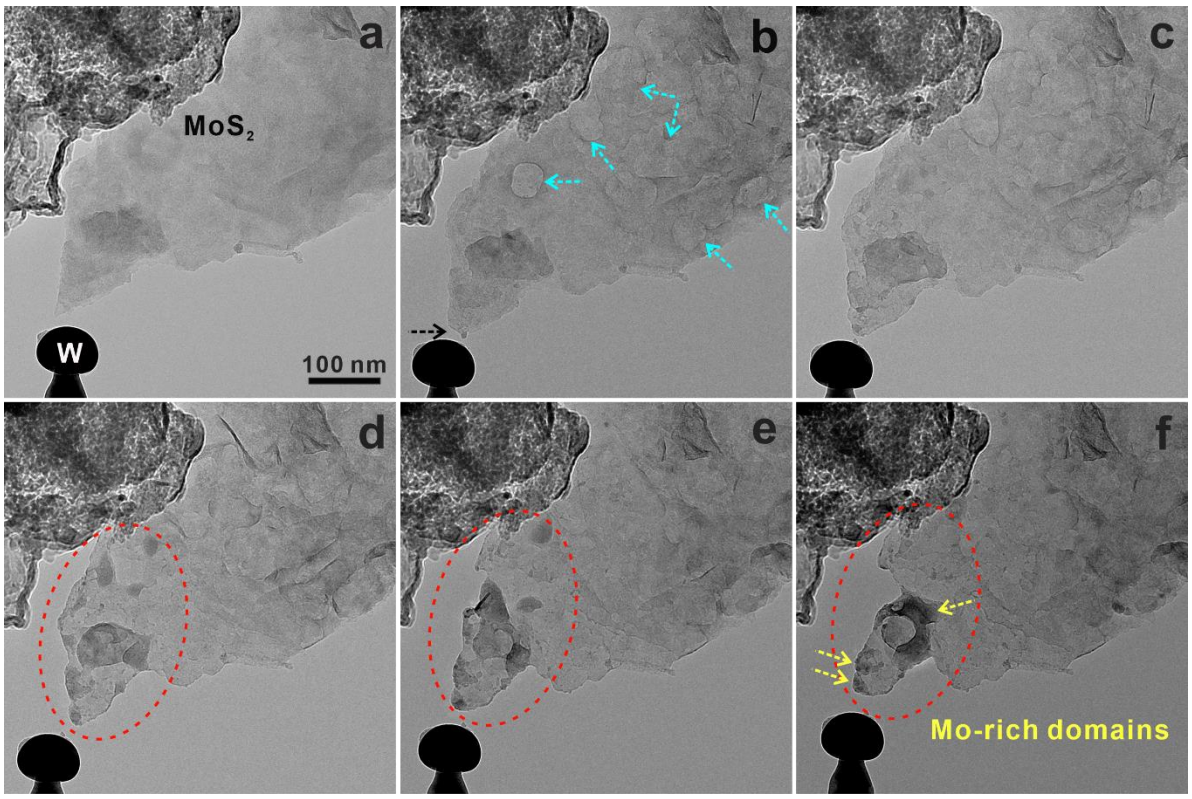

Figure S11. Structural evolution of a few-layered MoS_2 sheet during several tailoring attempts.

Figure S11 shows the structural evolution of a few-layered MoS_2 sheet during several tailoring attempts. As seen in Figure S11b, when the biased W tip touched the edge of a MoS_2 sheet, the sharp corner of the sheet was removed immediately, as marked by a black arrow. In the meantime, however, many holes were formed on the sheet surface, due to current-induced damage, as indicated by the blue arrows in Figure S11b. A few more contacts further altered the morphology of this MoS_2 sheet, and elemental segregation occurred in the circled region near the contact point (Figures S11d-f). The yellow arrows in Figure S11f indicate the Mo-rich zones or small particles that exhibit dark contrast, as confirmed by EDS analysis (not shown here). We also used the W tip capped with graphitic carbon to tailor MoS_2 sheets, which resulted in similar morphologies. In short, our method is not successful in tailoring MoS_2 sheets.

Supplementary Movies

Movie S1: *In situ* TEM observation of the tailoring process of a pure graphene sheet. (Displayed with ×10 speed of a real time process)

Movie S2: *In situ* TEM observation of the tailoring process of a RGO sheet. (Displayed with ×50 speed of a real time process)

Movie S3: *In situ* TEM observation of a single etching event in real time, which clearly shows that there is no physical contact between the sample and tip before the initiation of etching.

References

[1] Dresselhaus, M. S., Dresselhaus, G., Avouris, P., Eds.; *Carbon Nanotubes: Synthesis, Structure, Properties, and Applications;* Springer-Verlag: Berlin, Germany, 2001.